Planck constraint on relic primordial black holes

Steven J. Clark, Bhaskar Dutta, Yu Gao, Louis E. Strigari, and Scott Watson

Phys. Rev. D **95**, 083006 — Published 14 April 2017

DOI: 10.1103/PhysRevD.95.083006

MI-TH-1636, WSU-HEP-1609

Planck Constraint on Relic Primordial Black Holes

Steven J. Clark[1], Bhaskar Dutta[1], Yu Gao[1,2], Louis E. Strigari[1], and Scott Watson[3]
[1] *Department of Physics and Astronomy, Mitchell Institute for Fundamental Physics and Astronomy, Texas A&M University, College Station, TX 77843-4242, USA*
[2] *Department of Physics and Astronomy, Wayne State University, Detroit, MI 48201, USA*
[3] *Department of Physics, Syracuse University, Syracuse, NY 13244, USA*

We investigate constraints on the abundance of primordial black holes (PBHs) in the mass range $10^{15} - 10^{17}$ g using data from the Cosmic Microwave Background (CMB) and MeV extragalactic gamma-ray background (EGB). Hawking radiation from PBHs with lifetime greater than the age of the universe leaves an imprint on the CMB through modification of the ionization history and the damping of CMB anisotropies. Using a model for redshift dependent energy injection efficiencies, we show that a combination of temperature and polarization data from Planck provides the strongest constraint on the abundance of PBHs for masses $\sim 10^{15} - 10^{16}$ g, while the EGB dominates for masses $\gtrsim 10^{16}$ g. Both the CMB and EGB now rule out PBHs as the dominant component of dark matter for masses $\sim 10^{16} - 10^{17}$ g. Planned MeV gamma-ray observatories are ideal for further improving constraints on PBHs in this mass range.

I. INTRODUCTION

Shortly after the Big Bang, large density fluctuations in the early Universe may have resulted in the formation of primordial black holes (PBHs) [1]. There is a wide range of allowed masses for PBHs. Depending on the epoch and conditions during formation, PBH masses can be anywhere from approximately a gram to a million Solar masses. While low mass PBHs would have already evaporated through Hawking radiation [2], large ones with masses $M_{\rm BH} > 5 \times 10^{14}$ g would still be present today. It is also possible to have prolonged PBH formation during a non-radiation-dominated phase of the Universe where PBHs can form with a continuum mass distribution, rather than mostly at one particular mass scale as in the conventional radiation dominated case [3, 4]. Stable PBHs can be cosmologically-significant, and may serve as an ideal dark matter candidate [5].

Depending on the PBH abundance, Hawking radiation from PBHs with lifetimes longer than the age of the universe may be observable. Extragalactic gamma rays strongly constrain PBHs in the mass range $\sim 10^{15} - 10^{17}$ g [5]. PBHs in the mass range $\sim 10^{17} - 10^{20}$ g are bounded by femtolensing of gamma-ray bursts [6], and PBHs in the mass range $\sim 10^{-10} - 10$ $M_\odot$ are constrained by gravitational microlensing [7]. In addition, PBHs with mass $\gtrsim 10$ $M_\odot$ may be constrained by the accretion of matter in the early universe [8–10]. Black holes at approximately this mass are constrained by X-rays observations [11]. For recent comprehensive reviews on astrophysical constraints on PBHs see Refs. [12, 13].

In this paper we present a new bound on PBHs in the mass range $\sim 10^{15} - 10^{17}$ g using the most recent Planck Cosmic Microwave Background (CMB) data [14]. The CMB is sensitive to additional sources of energy injection during the recombination epoch, which leads to damping of the anisotropies. For PBHs, this energy injection is due to Hawking radiation. As we show, the Planck data now places a stronger bound on PBHs over a larger fraction of this mass range than the previous most stringent bounds derived from the extragalactic gamma-ray background (EGB). Previous authors have used Planck data to bound PBHs in the mass regime that we study [15]; as discussed below we precisely identify the mass regime over which the CMB and EGB bounds are dominant. In addition we note that our analysis is distinct from previous studies that used early-time distortions of the CMB to bound PBHs in the mass range $10^{11} - 10^{12}$ g [16].

The theoretical formalism that we utilize to constrain PBHs is similar to that used to constrain dark matter annihilation or decay [17–21]. From the perspective of the CMB, PBH evaporation is most similar to dark matter decay in that the energy injection only depends on the PBH mass and abundance, and is at a steady rate to the present time. This energy injection can have a significant impact on ionization at low redshift. However unlike the energy from dark matter, which can be injected in the form of heavy Standard Model particles, PBHs with mass $> 10^{15}$g mostly radiate in electrons and photons, or other (near) massless species, but generally not into much heavier particle species. Because PBHs with mass $> 10^{18}$g are too cold to emit electrons, their injection into the CMB is

unobservable, and the bounds are weak above this mass.

This paper is organized as follows. In Section II we briefly discuss the injection of radiation from PBHs. In Section III we discuss the impact of this injected energy on the IGM. In Section IV A, we show the modifications on the ionization history, and in Section IV B we discuss CMB distortions. In Section IV C we show the resulting constraints on PBHs, and Section V presents the discussion and conclusions.

II. BLACKHOLE RADIATION PROPERTIES

Depending on their mass, PBHs radiate a spectrum of particles, which decay via cascades into photons, electrons, protons, and neutrinos. These particles then deposit energy into the IGM. The injection of energy is described by the equation

$$\begin{aligned}\frac{dE}{dVdt} &= \dot{M}_{\rm BH}c^2 n_{\rm BH} \\ &= \frac{\dot{M}_{\rm BH}}{M_{\rm BH}}\rho_c c^2 \Omega_{\rm BH}(z) \\ &= \frac{\dot{M}_{\rm BH}}{M_{\rm BH}}\rho_c c^2 \Omega_{\rm BH,0}(1+z)^3,\end{aligned} \tag{1}$$

where $n_{\rm BH}$ is the PBH number density, ρ_c is the critical density of the Universe today, $M_{\rm BH}$ is the PBH mass, $\Omega_{\rm BH}(z)$ is the PBH density relative to the critical density, and $\Omega_{\rm BH,0}$ is the value of $\Omega_{\rm BH}(z)$ today.

Note that the above equations assume that PBHs are comprised of a single mass and the mass does not changes as it radiates. This is satisfied as long as the lifetime is large compared to the age of the universe and is satisfied by the masses considered in this work. Apart from some cosmetic differences, Equation (1) is identical to that for decaying dark matter [22].

In order to evaluate Equation (1), an expression for $\dot{M}_{\rm BH}$ is required. To obtain this, we start from the fact that Hawking radiation equates the radiation from a black hole to the blackbody radiation of an object with temperature

$$T_{\rm BH} = \frac{1}{8\pi G M} = 1.06{\rm TeV} \times \frac{10^{10}{\rm g}}{{\rm M_{BH}}} \tag{2}$$

and with an emission spectrum

$$\frac{dN}{dEdt} \propto \frac{\Gamma_s}{e^{E/T_{\rm BH}} - (-1)^{2s}} \tag{3}$$

where s is the spin of the radiated particle and Γ_s is the absorption coefficient for the particle. For low $T_{\rm BH}$ the absorption coefficient can deviate greatly from the geometric optic limit [23],

$$\Gamma_s(M,E) = \frac{27G^2M^2E^2}{\hbar^2c^6}. \tag{4}$$

Hawking radiation causes black holes to lose mass at a rate [5, 23]

$$\dot{M}_{\rm BH} = -5.34\times10^{25} F(M_{\rm BH}) M_{\rm BH}^{-2}\,{\rm g}^3\,{\rm s}^{-1}. \tag{5}$$

where $F(M_{\rm BH})$ is a measure of the fraction of emitted particles normalized to unity for $M_{\rm BH} \gg 10^{17}$ g, and evaluated by summing over the various particles.

$$F(M_{\rm BH}) = \left(\sum_i f_i\right) \tag{6}$$

The fractions for particles of different spins emitted in the region of interest are [23]

$$\begin{aligned} f_0 = 0.267, \quad f_1^\gamma = 0.06, \quad f_{3/2} = 0.02, \\ f_2^g = 0.007, \; f_{1/2}^\nu = 0.147, \; f_{1/2}^{e\pm} = 0.142. \end{aligned} \tag{7}$$

Since only the electrons and photons interact electromagnetically for the PBH masses considered, these are the only fractions that need to be considered for calculating the energy output.

III. MEDIUM INTERACTIONS

The energy deposited into the IGM by PBHs is absorbed through multiple channels. Following previous studies, we consider three channels for the IGM interaction: Hydrogen ionization, Lyman-Alpha excitations, and heating the IGM [21, 27, 28]. These effects alter the cosmological recombination equations as

$$\frac{dx_e}{dz} = \left(\frac{dx_e}{dz}\right)_{\rm orig} - \frac{1}{(1+z)H(z)}(I_{Xi}(z) + I_{X\alpha}(z)) \tag{8}$$

$$\frac{dT_{\rm IGM}}{dz} = \left(\frac{dT_{\rm IGM}}{dz}\right)_{\rm orig} - \frac{2}{3k_B(1+z)H(z)}\frac{K_h}{1+f_{\rm He}+x_e}, \tag{9}$$

where $f_{\rm He}$ is the helium fraction, x_e is the ionization fraction, k_B is the Boltzmann constant, and $H(z)$ is the Hubble parameter. The standard equations without additional energy injection from PBHs are denoted by the subscript "orig" and are derived in e.g. Ref. [29]. The quantities $I_{Xi}(z)$, $I_{X\alpha}(z)$, and K_h are factors corresponding to the additional energy injection affecting ionization from the ground state, ionization from excited states, and heating the IGM. Each of these injections are dependent on the injection energy through

$$I_{Xi}(z) = f_i(E,z)\frac{dE/dVdt}{n_H(z)E_i} \tag{10}$$

$$I_{X\alpha}(z) = f_\alpha(E,z)(1-C)\frac{dE/dVdt}{n_H(z)E_\alpha} \tag{11}$$

$$K_h(z) = f_h(E,z)\frac{dE/dVdt}{n_H(z)}. \tag{12}$$

Here n_H is the hydrogen number density, and E_i and E_α are the energies of the ground and the excited hydrogen atom electron levels respectfully. The quantity C is related to the probability for an excited hydrogen atom to emit a photon prior to being ionized [18]. The quantities $f_i(E,z)$, $f_\alpha(E,z)$, $f_h(E,z)$ are efficiencies for energy interactions through each channel. Commonly referred to as effective efficiencies, they are redshift, energy, and species dependent quantities that equate the total energy injection to the actual amount absorbed through a pathway [21]. Previously, these efficiencies have been approximated by simple x_e dependent equations, with the energy injection taken to be instantaneous, through a technique known as the "SSCK" method, described in further detail in Ref. [18, 19].

To calculate the effective efficiencies, we follow the approach adopted in Ref. [20, 21]. These efficiencies have been tabulated for electron and photon particle injection into the IGM at various redshifts and particle energies, and divided into five different channels: Hydrogen ionization, Helium ionization, Lyman-alpha excitations, heating, and continuum photons (energy lost as photons with $E < 10.2\,\text{eV}$) [20]. The Hydrogen, Lyman-alpha, and heating efficiencies were used to calculate the various efficiencies in Equations (10), (11), and (12). We do not consider Helium ionization because it is subdominant.

We additionally note that we do not consider energy deposited into continuum photons. This is because continuum photon energy affects the CMB mostly through spectral distortions rather than through anisotropies, and the anisotropies are the focus of this paper. The impact on spectral distortions is also less significant than on anisotropies [20]; a basic demonstration of this is given in the Appendix.

Refs. [20, 21] tabulate efficiencies specifically for decaying and annihilating dark matter into electron and photon channels. These efficiencies are specifically valid for a small ionization fraction, in which case the efficiency scales linearly with ionization fraction. For dark matter decay, the energy injection is linearly proportional to the density, and for annihilation it is proportional to the density-squared. From Equation (1), the radiation from PBHs is linearly proportional to density, therefore this is most analogous to dark matter decay. For this reason, we utilize the decay efficiencies to produce black hole efficiencies. To obtain the PBH efficiency from individual particle efficiencies, we assume that PBH injected particles have the same spectrum as the high energy limit, Equation (3). Then combining the various efficiencies for different energies and species through a weighted average based upon their emission fractions gives

$$f_{c,\rm BH}(M_{\rm BH},z) = \frac{\sum_i \int_0^\infty g_i f_i f_{c,i}(E,z)\left(\frac{dN}{dEdt}(E)\right)_i dE}{\sum_i \int_0^\infty g_i f_i \left(\frac{dN}{dEdt}(E)\right)_i dE} \tag{13}$$

where $f_{c,\rm BH}(M_{\rm BH},z)$ and $f_{c,i}(E,z)$ are the black hole and other particles denoted by i effective efficiencies for a specific energy where c denotes the interaction channel being considered, ie. Hydrogen ionization. g_i and f_i are the degeneracy and emission fraction of particle i defined in Equation (7).

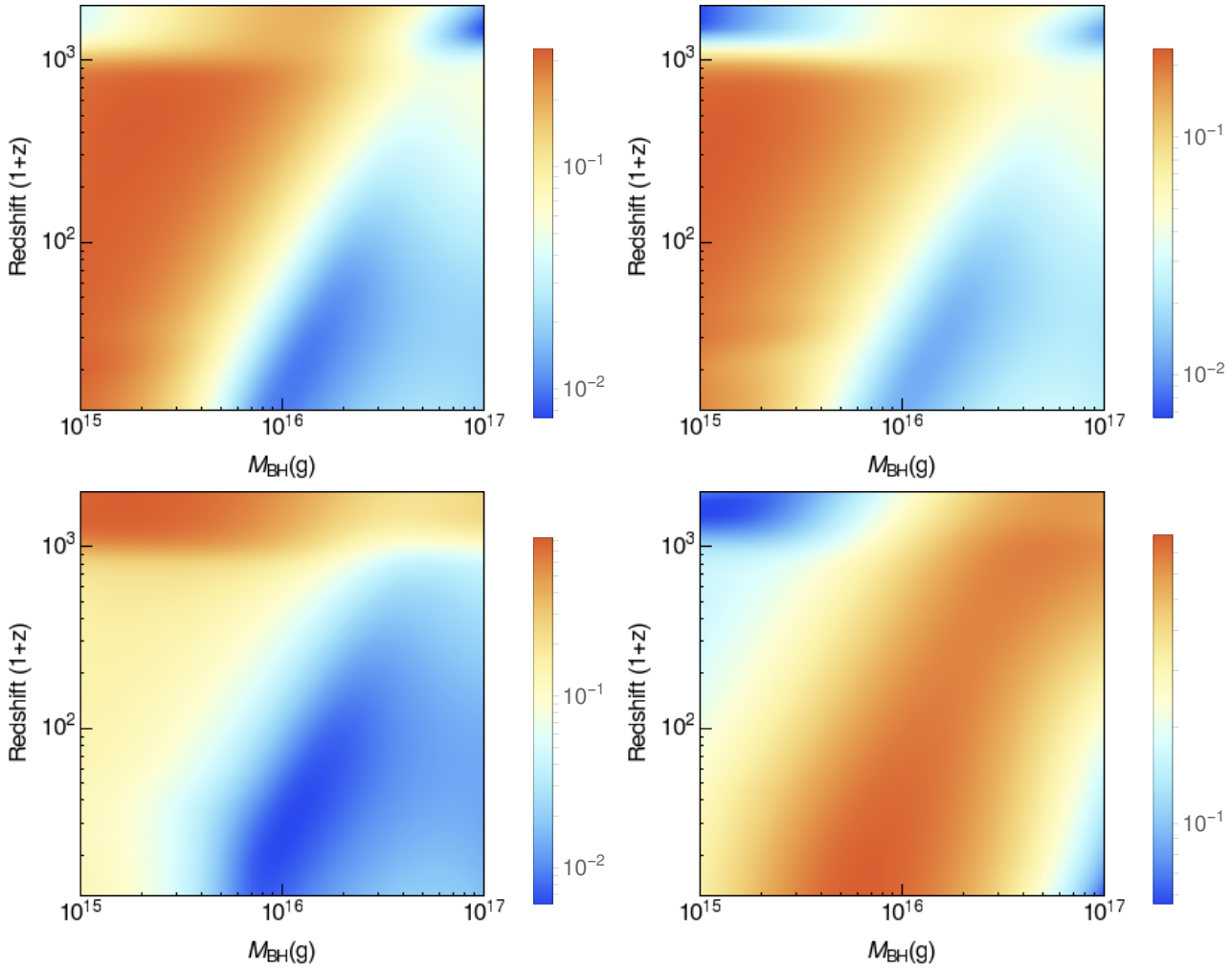

FIG. 1: Effective efficiencies of energy deposition from black holes that release electrons and photons in the manner described in Section II. From left to right, top to bottom, the curves are - Hydrogen Ionization, Lyman-Alpha Excitations, Heating, and Continuum Photons

Using the decay efficiencies from Refs. [20, 21], Figure 1 shows the effective efficiencies for PBH Hawking radiation for the mass range considered in this work. It should be noted that there appears a location where the efficiency drops drastically for all channels used in altering the ionization history, and this location shifts to earlier times for increasing masses. This drop will have a direct impact on the constraints for a given PBH mass. For ease of reference, Figure 2 contains the effective efficiencies for a few select PBH masses. These efficiencies are comparable but distinct from those shown in Ref. [15]. While we both applied similar methods in calculating the effective efficiencies, a key difference arose in estimating the black hole emission spectrum. Because the majority of the contribution arises from the high end of the spectrum, no significant differences were found between treating the entire spectrum at the high energy limit or including a sufficiently low minimum cutoff energy.

IV. RESULTS

To model the energy injection from PBHs and its impact on the recombination history and CMB, we utilize the CAMB [30, 31] and HYREC [29] codes. We incorporate two new parameters into the code, the PBH mass, $m_{\rm BH}$, and the ratio of the PBH density to the total dark matter density, $\Omega_{\rm BH}/\Omega_{\rm DM}$. With this modification to the recombination history, we fit CMB data using the COSMOMC code [32, 33]. We varify that with these modifications we are able to reproduce the results previously calculated for dark matter decay [21]. In Section IV A we determine how PBH energy injections alter the ionization history, in Section IV B we determine the general effects the energy injection has on CMB anisotropies, and in Section IV C we present constraints on the PBH density.

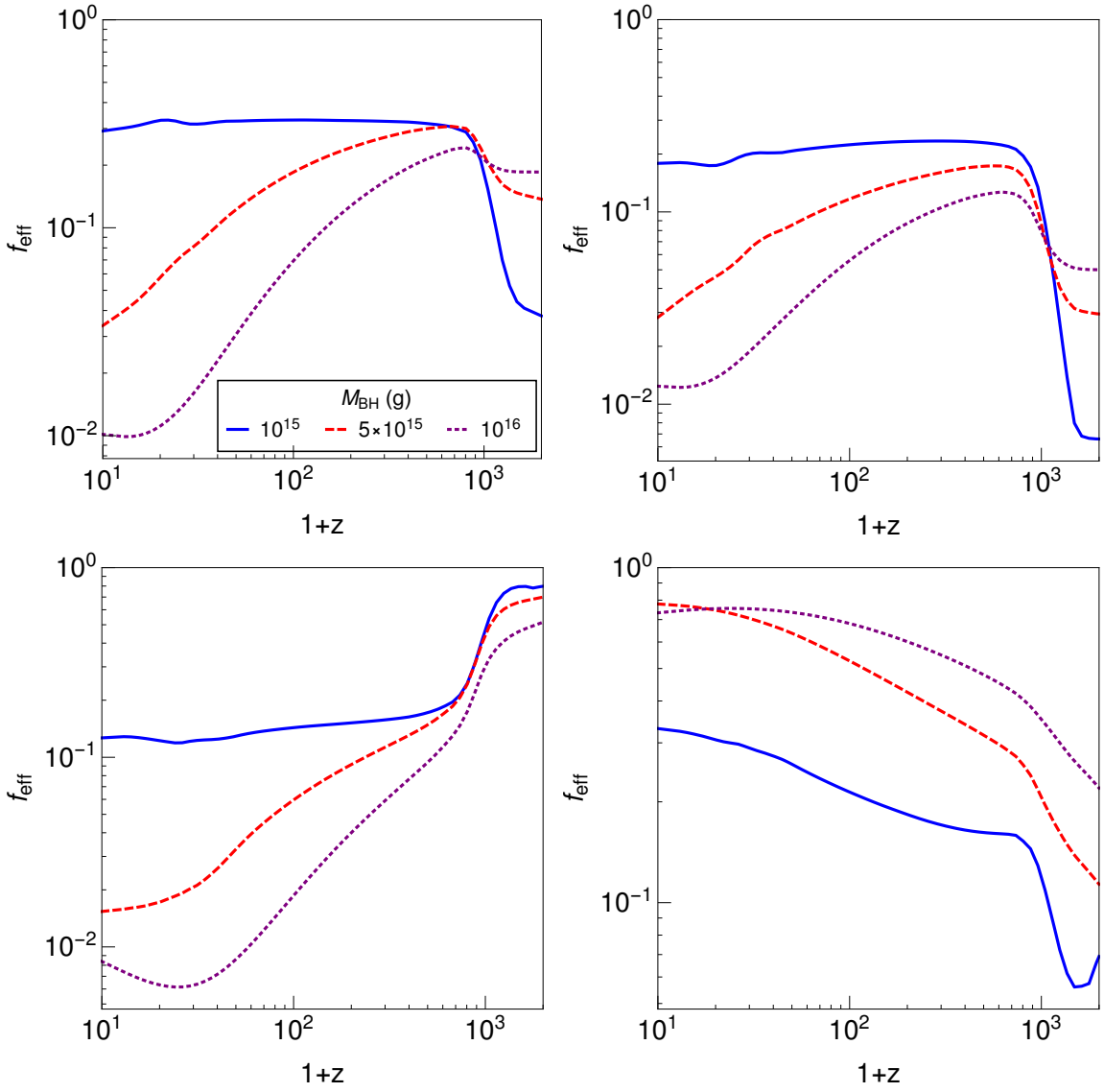

FIG. 2: Effective efficiencies of energy deposition from black holes for a few specific masses. From left to right, top to bottom, the curves are - Hydrogen Ionization, Lyman-Alpha Excitations, Heating, and Continuum Photons

A. Recombination History

The alterations to x_e and $T_{\rm IGM}$ are shown for a few example PBH masses in Figure 3. The percent change relative to the standard model with no PBHs is indicated. Figure 3 shows that there is only a minor variation relative to the no PBH case in both x_e and $T_{\rm IGM}$ at large redshifts, with the significant deviations only apparent at $\sim z = 200 - 300$. The minimal deviation at high redshift supports the use of the effective efficiencies [19]. For standard values of the cosmological parameters, x_e and $T_{\rm IGM}$ are both well below the observational limits on these quantities [24–26],

$$\begin{aligned} x_e(z\sim 7) &= 0.66^{+0.12}_{-0.09} & x_e(z\sim 8) &< 0.35 \\ \log_{10}(T_{\rm IGM}(z=4.8)) &= 3.9\pm 0.1 & \log_{10}(T_{\rm IGM}(z=6.08)) &= 4.21^{+0.06}_{-0.07}. \end{aligned} \tag{14}$$

We note that contributions from reionization and structure formation are not included in this calculation, though it may be possible that PBHs around the masses that we study can represent a significant contribution to reionization [27].

Since there is a large variation in the ionization fraction at later times, assumptions made about the effective efficiencies weaken. In order to observe possible errors introduced due to this large deviation, an ionization history

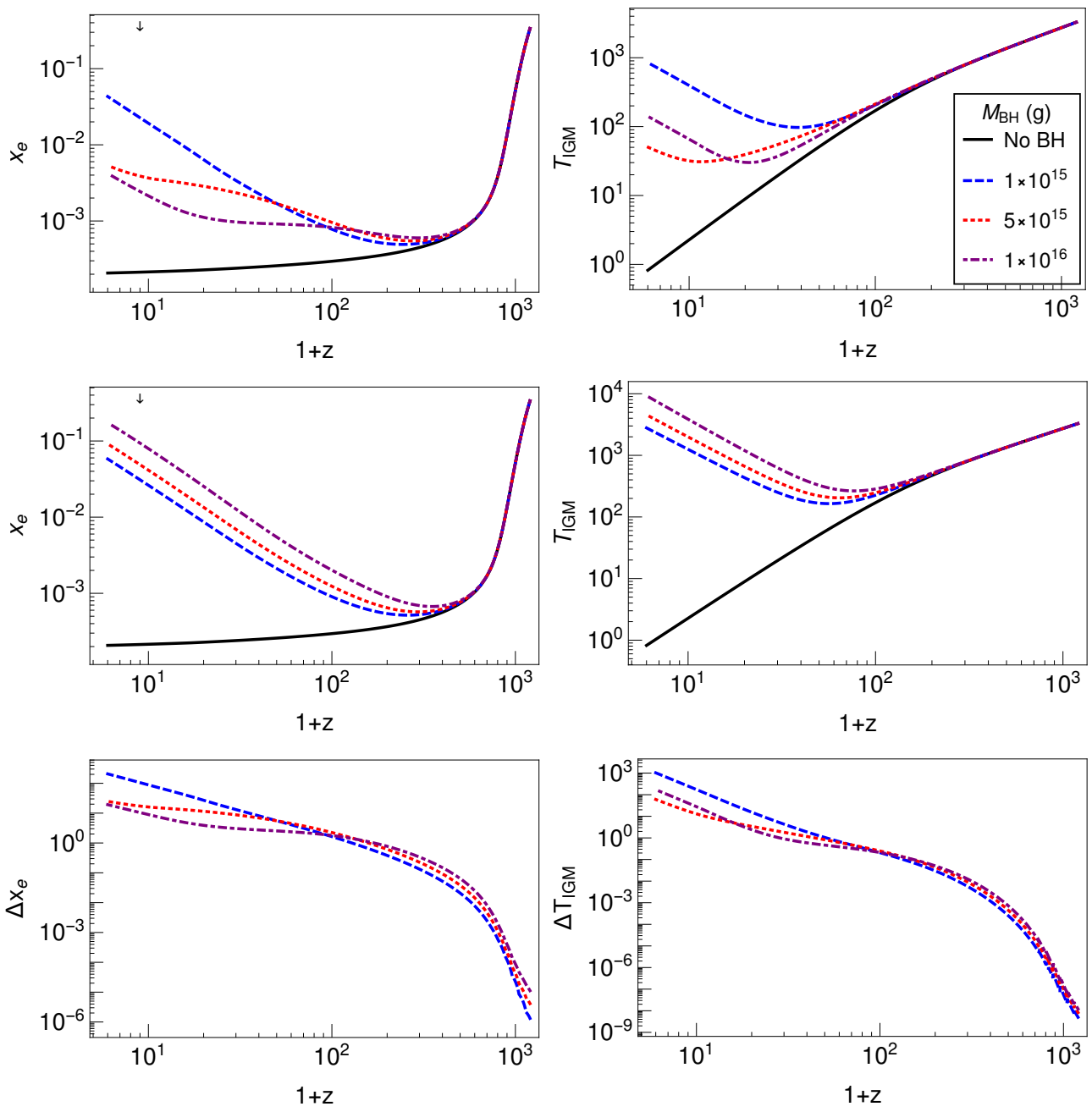

FIG. 3: Ionization fraction (left) and temperature of the IGM (right) due to PBH energy injection using effective efficiencies (top), using the "SSCK" prescription (middle), and percent change from the no PBH case (bottom). Bounds on the parameters are also plotted. The PBH density $\Omega_{\rm BH}$ for each mass is taken to be at the 95% confidence limit discussed in this work. The legend applies to all graphs.

developed using the "SSCK" prescription [18, 19] and the same cosmological parameters is also given in Figure 3. While there is again a large variation at late times, up to two orders of magnitude, x_e and $T_{\rm IGM}$ are still far below the observational constraints. Additionally during the period of interest at high redshift, they have only minor variation relative to the standard no PBH case.

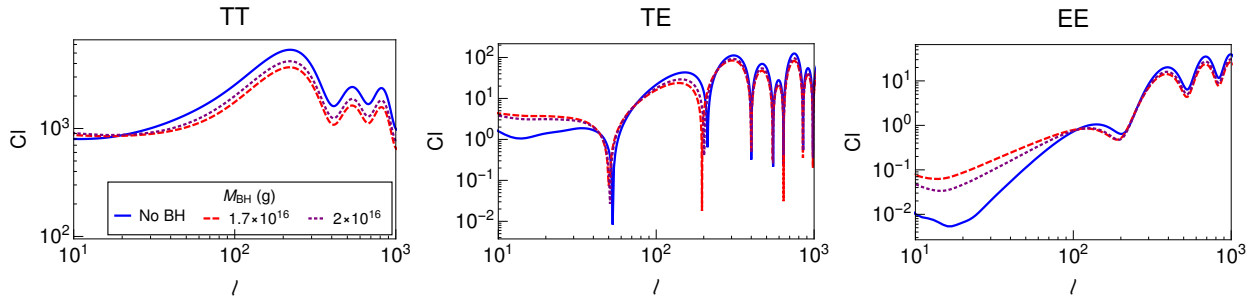

FIG. 4: Effect that various PBH masses have on the CMB for TT (left), TE (middle), and EE (right) correlations. The legend present in the TT panel also applies to the TE and EE panels.

B. CMB Anisotropies

PBHs also affect the measured CMB anisotropy power spectrum. Here we discuss the affect on the Temperature-Temperature (TT), Temperature-(E-mode) (TE), and (E-mode)-(E-mode) (EE) power spectra. In Figure 4, TT, TE, and EE correlations are given for example PBH masses, assuming $\Omega_{\rm BH}$ composes all of the dark matter. As can be expected, larger changes arise from smaller mass PBHs due to both their larger radiation rate as well as their higher number density at equal mass densities.

The energy injection results in a scale-dependent deviation from the standard case with no PBHs; there is an increase in the power spectrum at small multipoles and a decrease at large multipoles. This behavior can be understood by noting that the width of the last scattering surface increases because of the PBH energy injection. Perturbations on scales smaller than the width of the last scattering surface are suppressed, as can be most easily seen for TT correlations. In addition the TE and EE spectra shift with an energy injection. These shifts are due to the increased contributions by monopole perturbations which trace to polarization and are introduced with the increased width of the scattering surface [34].

C. PBH constraints

To place constraints on the abundance of PBHs, we fit the simulated spectra to Planck half mission data [14]. The likelihood used was TT, TE, EE+lowP, a combination of TT, TE, and EE correlations as well as B-mode correlations for $l \leq 29$. Figure 5 shows the posterior probability densities for a few example cosmological parameters, both with and without PBHs. As can be seen, the distributions are consistent with each other, up to minor shifts well within experimental uncertainties. Note that this has been highlighted in previous studies of the impact of dark matter annihilation and decay on the CMB [22].

Since there is little variation in the base cosmological parameters, for computational convenience to set upper limits on $\Omega_{\rm BH}$ we take the six principal cosmological parameters to be fixed at their best fit values in the case of no additional energy injection [35]. The six principal cosmological parameters are: the physical baryon density, $\Omega_b h^2$; the physical CDM matter density, $\Omega_c h^2$; the CMB acoustic scale parameter, $100\theta_{\rm MC}$; the reionization optical depth, τ; primordial curvature perturbations, $\ln(10^{10}{\rm A_s})$; and the scalar spectral index, n_s [36]. Figure 6 shows the result of the 95% confidence limit, where the confidence limit is defined as the cumulative distribution centered around the median, which corresponds closely to the peak of the distributions in Figure 6. The constraint follows the expected inverse cube relationship to the PBH mass which is predicted by the energy injection formula.

In addition to the cubic dependence on mass, there is also a highly nonlinear relationship to the effective efficiency. This nonlinearity is most prevalent at a PBH mass around $1 - 4 \times 10^{16}$ g. Comparing effective efficiencies, in Figure 1, the trend is correlated with the efficiency values that occur near the time of recombination. As the efficiency value decreases, it is required for a larger amount of total energy to be created in order to produce the same effect. For this reason, as the efficiency experiences a large decrease in this mass range, the allowable maximum mass fraction increases. This nonlinear behavior is also observed in [15] to a much lesser degree.

We note that since the six base cosmological parameters were fixed, the PBH abundance may be more strongly constrained than in a model in which more parameters are allowed to vary. To check this, we compare to the case in which the base cosmological parameters are allowed to vary for a single PBH mass of 2×10^{16} g. We find that by freeing all of the cosmological parameters, the constraint on $\Omega_{\rm BH}$ may be weakened by up to a factor of three. However, as stated above for computational convenience we have decided to fix the base cosmological parameters for

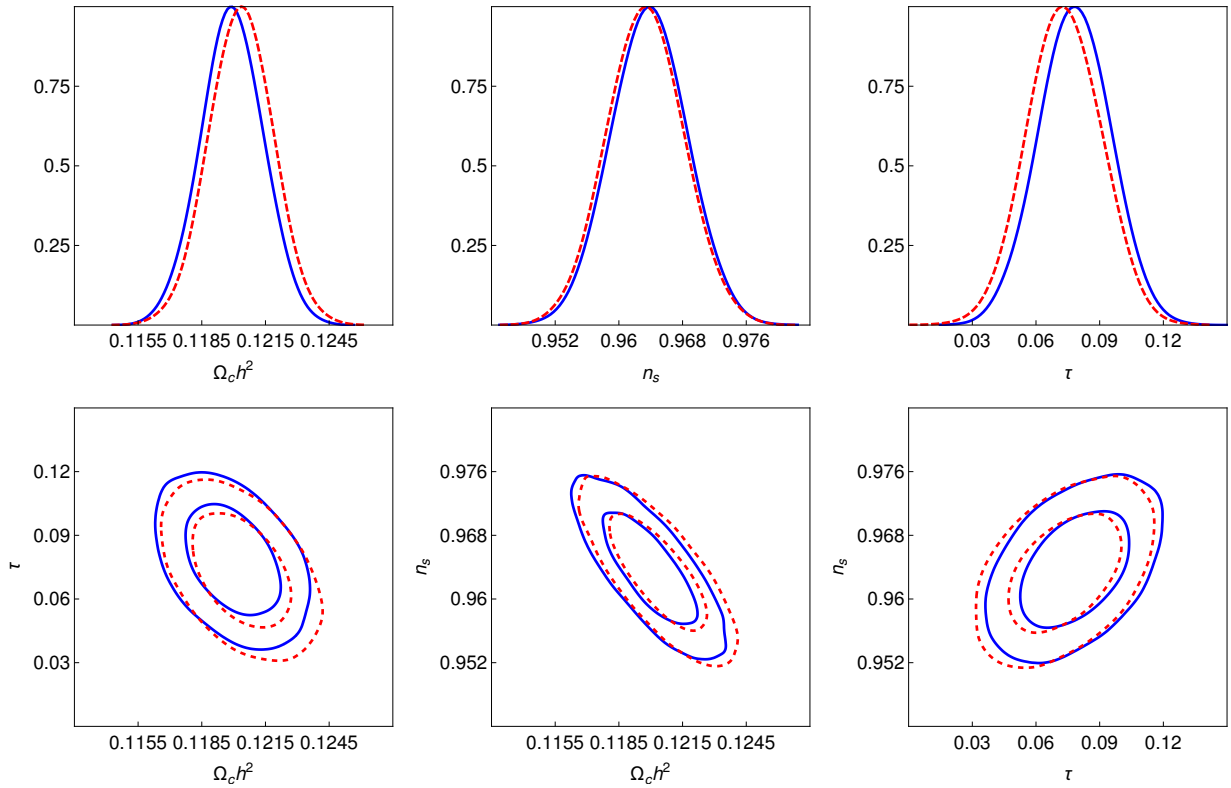

FIG. 5: Change in the posterior probability distributions for a few principal cosmological parameters for PBHs of mass $2\times10^{16}g$. The optical depth is τ and the spectral index is n_s. *Top row*: Single variable distributions with most probable values normalized to one, where blue (solid) lines represent no PBH case while red (dashed) includes PBHs. *Bottom row*: Correlations between different parameters, with inner and outer curves correspond to 68% and 95% confidence levels respectfully.

our main bounds on Ω_{BH}.

As indicated above, previous analyses have used the EGB to constrain PBHs in the mass regime $10^{15}-10^{17}$ g [5, 12]. Since PBHs emit a mass-dependent gamma-ray spectrum, there is an upper bound on their density before they would be excluded by EGB measurements. Following the prescription outlined in Ref. [5], the number density of photons $n_{\gamma 0}$ with energy $E_{\gamma 0}$ and their intensity is

$$n_{\gamma 0}(E_\gamma) = \frac{\Gamma_{\rm BH}}{M_{\rm BH}} E_\gamma \int_{t_{\rm min}}^{\min(t_0,\tau)} dt(1+z)^{-2} \frac{\dot{N}_\gamma}{E_\gamma}(M_{\rm BH},(1+z)E_\gamma) \tag{15}$$

$$I = \frac{c}{4\pi} n_{\gamma 0} \tag{16}$$

where $t_{\rm min}$ is the time when photon creation begins. The quantity $\dot{N}_\gamma/E_\gamma(M_{\rm BH},E_\gamma)$ is the photon spectrum given by Equation (3), which we take at the high energy limit. For PBHs in the mass range studied, peak intensity occurs at $\sim 1-30$ MeV. Constraints were derived by matching the intensity to the upper bound of the COMPTEL EGB experimental data [37].

EGB constraints are also shown in Figure 6 as well as those imposed by femtolensing [12]. We find that Planck provides the strongest constraint on the abundance of PBHs for masses $\sim 10^{15}-10^{16}$ g, while the EGB dominates for masses $\gtrsim 10^{16}$ g. Note that while using a similar approach, this conclusion differs from that of Ref. [15]. A comparison of the two limits is shown after the Appendex in Figure 8. The Planck constraint deviates from a linear relation because of the model for effective efficiencies.

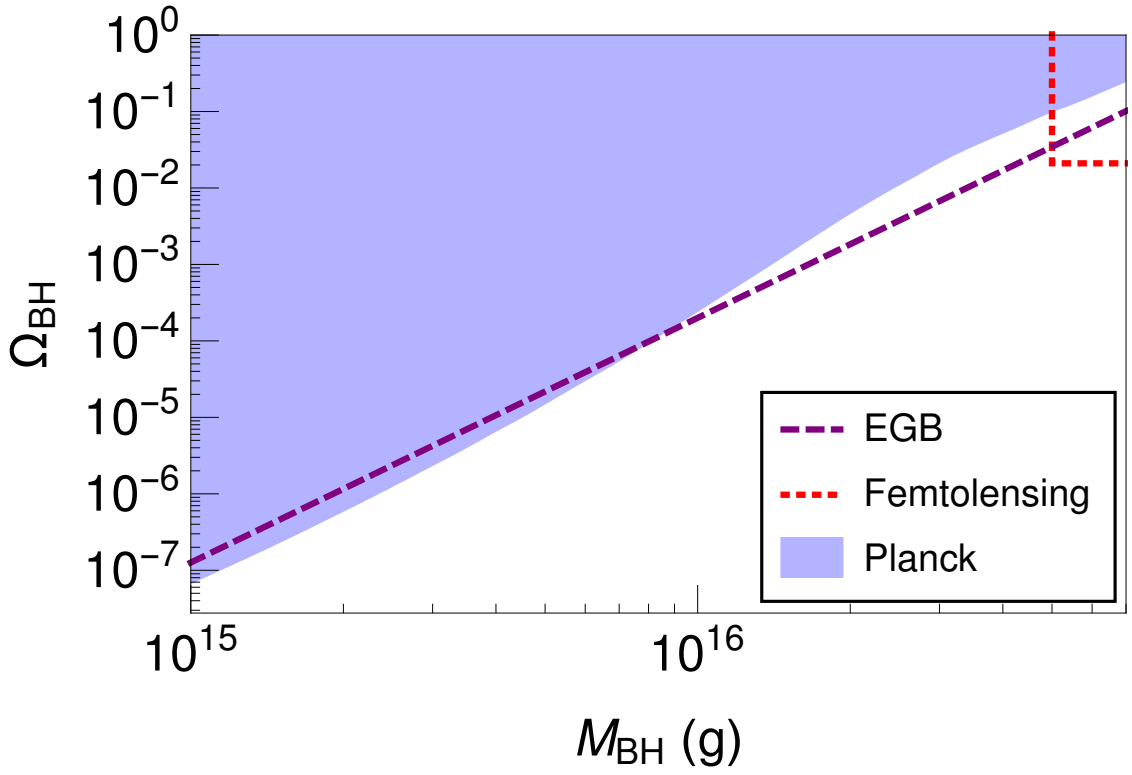

FIG. 6: CMB exclusion bounds for $\Omega_{\rm BH}$ at the 95% confidence level (shaded region) compared with the same exclusion bound enforced by EGB, assuming 100% of the background produced by PBHs (long dashes). Also included is an estimation for the bound that is imposed due to femtolensing (short dashes) considered in [12] and an approximation of the bound found in [15] (long-short dashes.

V. CONCLUSIONS

PBHs are of great interest in cosmology. They reveal conditions in the early universe and can serve as a dark matter candidate. There are several standard mechanisms that have been proposed to detect PBHs; these include detection of Hawking radiation, detection of radiation produced from accretion disks, and gravitational lensing. Each method is capable of targeting different PBH mass ranges. In this paper, we have focused on PBHs with masses in the range $10^{15} - 10^{17}$ g. We have improved and made more precise the constraints in this mass range using the CMB and EGB. For our CMB bound, we model the energy absorption not as instantaneous, but rather using redshift dependent efficiency. The energy injection results in an increase in the ionization fraction at late times as well as an increase in the IGM temperature, leading to distortions of the CMB anisotropies. Larger fractional changes occur at large multipoles because of the increase of the width of the last scattering surface.

Using Planck data, we show that CMB distortions from Hawking radiation allow for stringent constraints on the density of $10^{15} - 10^{17}$ g PBHs of $\Omega_{\rm BH} \lesssim 3.3 \times 10^{-9} (m_{\rm BH}/M_\star)^{3.8}$. We show that for mass $\sim 10^{15} - 10^{16}$ g, the CMB constraints are stronger than the constraints from the $\sim 1-30$ MeV EGB, which imply, $\Omega_{\rm BH} \lesssim 1.4 \times 10^{-8} (m_{\rm BH}/M_\star)^{3.2}$. Constraints imposed by CMB spectral distortions from Hawking radiation producing sub 10.2 eV photons are also much weaker than our constraint.

In the future, our theoretical analysis may be improved by including a mass spectrum of PBHs. In addition, even though we have used the EGB to bound the contribution of PBHs, it may be interesting to consider the EGB as a signal of PBHs. This is an exciting possibility because the origin of this $\sim$ MeV gamma-ray background is not yet known [39–41]. Future missions to measure MeV gamma-rays will be especially important for the study of PBHs [42].

Acknowledgements

The authors thank Daniel Meerburg for helpful discussion and modified HyREC codes. We also thank Tomohiro Harada and Tracy Slatyer for helpful discussions. BD acknowledges support from DOE Grant DE-FG02-13ER42020.

LES acknowledges support from NSF grant PHY-1522717. YG thanks the Mitchell Institute for Fundamental Physics and Astronomy and Wayne State University for support. SC acknowledges support from NASA Astrophysics Theory grant NNX12AC71G. SW is supported in part by NASA Astrophysics Theory Grant NNH12ZDA001N and DOE grant DE-FG02-85ER40237. The authors acknowledge the Texas A&M University Brazos HPC cluster that contributed to the research reported here. <brazos.tamu.edu>

[1] S. Hawking, Mon. Not. Roy. Astron. Soc. **152**, 75 (1971).
Y. B. Zel'dovich, I. D. Novikov, Astron. Zh. volume 43, pages 758, 1966;
Y. B. Zel'dovich, I. D. Novikov, Sov. Astron. volume 10, pages 602, 1967.
B. J. Carr and S. W. Hawking, Mon. Not. Roy. Astron. Soc. **168**, 399 (1974).
[2] S. W. Hawking, Nature **248**, 30 (1974). doi:10.1038/248030a0
[3] J. Georg, G. Sengor, and S. Watson, Phys. Rev. D **93**, no. 12, 123523 (2016) doi:10.1103/PhysRevD.93.123523 [arXiv:1603.00023 [hep-ph]].
[4] T. Harada, C. M. Yoo, K. Kohri, K. i. Nakao and S. Jhingan, Astrophys. J. **833**, no. 1, 61 (2016) doi:10.3847/1538-4357/833/1/61 [arXiv:1609.01588 [astro-ph.CO]].
[5] B. J. Carr, K. Kohri, Y. Sendouda and J. Yokoyama, Phys. Rev. D **81**, 104019 (2010) doi:10.1103/PhysRevD.81.104019 [arXiv:0912.5297 [astro-ph.CO]].
[6] R. J. Nemiroff, G. F. Marani, J. P. Norris and J. T. Bonnell, Phys. Rev. Lett. **86**, 580 (2001) doi:10.1103/PhysRevLett.86.580 [astro-ph/0101488].
[7] K. Griest, A. M. Cieplak and M. J. Lehner, Phys. Rev. Lett. **111**, no. 18, 181302 (2013). doi:10.1103/PhysRevLett.111.181302
[8] M. Ricotti, J. P. Ostriker and K. J. Mack, Astrophys. J. **680**, 829 (2008) doi:10.1086/587831 [arXiv:0709.0524 [astro-ph]].
[9] L. Chen, Q. G. Huang and K. Wang, arXiv:1608.02174 [astro-ph.CO].
[10] Y. Ali-HaÂŢmoud and M. Kamionkowski, arXiv:1612.05644 [astro-ph.CO].
[11] D. Gaggero, G. Bertone, F. Calore, R. M. T. Connors, M. Lovell, S. Markoff and E. Storm, arXiv:1612.00457 [astro-ph.HE].
[12] B. Carr, F. Kuhnel and M. Sandstad, Phys. Rev. D **94**, no. 8, 083504 (2016) doi:10.1103/PhysRevD.94.083504 [arXiv:1607.06077 [astro-ph.CO]].
[13] A. M. Green, Phys. Rev. D **94**, no. 6, 063530 (2016) doi:10.1103/PhysRevD.94.063530 [arXiv:1609.01143 [astro-ph.CO]].
[14] N. Aghanim *et al.* [Planck Collaboration], Astron. Astrophys. **594**, A11 (2016) doi:10.1051/0004-6361/201526926 [arXiv:1507.02704 [astro-ph.CO]].
[15] V. Poulin, J. Lesgourgues and P. D. Serpico, arXiv:1610.10051 [astro-ph.CO].
[16] H. Tashiro and N. Sugiyama, Phys. Rev. D **78**, 023004 (2008) doi:10.1103/PhysRevD.78.023004 [arXiv:0801.3172 [astro-ph]].
[17] L. Zhang, X. Chen, M. Kamionkowski, Z. g. Si and Z. Zheng, Phys. Rev. D **76**, 061301 (2007) doi:10.1103/PhysRevD.76.061301 [arXiv:0704.2444 [astro-ph]].
[18] M. S. Madhavacheril, N. Sehgal and T. R. Slatyer, Phys. Rev. D **89**, 103508 (2014) doi:10.1103/PhysRevD.89.103508 [arXiv:1310.3815 [astro-ph.CO]].
[19] T. R. Slatyer, Phys. Rev. D **93**, no. 2, 023527 (2016) doi:10.1103/PhysRevD.93.023527 [arXiv:1506.03811 [hep-ph]].
[20] T. R. Slatyer, Phys. Rev. D **93**, no. 2, 023521 (2016) doi:10.1103/PhysRevD.93.023521 [arXiv:1506.03812 [astro-ph.CO]].
[21] H. Liu, T. R. Slatyer and J. Zavala, Phys. Rev. D **94**, no. 6, 063507 (2016) doi:10.1103/PhysRevD.94.063507 [arXiv:1604.02457 [astro-ph.CO]].
[22] T. R. Slatyer and C. L. Wu, arXiv:1610.06933 [astro-ph.CO].
[23] J. H. MacGibbon and B. R. Webber, Phys. Rev. D **41**, 3052 (1990). doi:10.1103/PhysRevD.41.3052;
J. H. MacGibbon, Phys. Rev. D **44**, 376 (1991). doi:10.1103/PhysRevD.44.376
[24] J. S. Bolton, G. D. Becker, S. Raskutti, J. S. B. Wyithe, M. G. Haehnelt and W. L. W. Sargent, doi:10.1111/j.1365-2966.2011.19929.x arXiv:1110.0539 [astro-ph.CO].
[25] J. S. Bolton, G. D. Becker, J. S. B. Wyithe, M. G. Haehnelt and W. L. W. Sargent, Mon. Not. Roy. Astron. Soc. **406**, 612 (2010) doi:10.1111/j.1365-2966.2010.16701.x [arXiv:1001.3415 [astro-ph.CO]].
[26] M. A. Schenker, R. S. Ellis, N. P. Konidaris and D. P. Stark, Astrophys. J. **795**, no. 1, 20 (2014) doi:10.1088/0004-637X/795/1/20 [arXiv:1404.4632 [astro-ph.CO]].
[27] K. M. Belotsky and A. A. Kirillov, JCAP **1501**, no. 01, 041 (2015) doi:10.1088/1475-7516/2015/01/041 [arXiv:1409.8601 [astro-ph.CO]].
[28] T. R. Slatyer, Phys. Rev. D **87**, no. 12, 123513 (2013) doi:10.1103/PhysRevD.87.123513 [arXiv:1211.0283 [astro-ph.CO]].
[29] Y. Ali-Haimoud and C. M. Hirata, Phys. Rev. D **83**, 043513 (2011) doi:10.1103/PhysRevD.83.043513 [arXiv:1011.3758 [astro-ph.CO]].
[30] A. Lewis, A. Challinor and A. Lasenby, Astrophys. J. **538**, 473 (2000) doi:10.1086/309179 [astro-ph/9911177].
[31] C. Howlett, A. Lewis, A. Hall and A. Challinor, JCAP **1204**, 027 (2012) doi:10.1088/1475-7516/2012/04/027 [arXiv:1201.3654 [astro-ph.CO]].
[32] A. Lewis, Phys. Rev. D **87**, no. 10, 103529 (2013) doi:10.1103/PhysRevD.87.103529 [arXiv:1304.4473 [astro-ph.CO]].
[33] A. Lewis and S. Bridle, Phys. Rev. D **66**, 103511 (2002) doi:10.1103/PhysRevD.66.103511 [astro-ph/0205436].

[34] N. Padmanabhan and D. P. Finkbeiner, Phys. Rev. D **72**, 023508 (2005) doi:10.1103/PhysRevD.72.023508 [astro-ph/0503486].
[35] "Planck 2015 Results: Cosmological Parameter Tables," `https://wiki.cosmos.esa.int/planckpla2015/images/6/67/Params_table_2015_limit68.pdf`
[36] P. A. R. Ade *et al.* [Planck Collaboration], Astron. Astrophys. **571**, A16 (2014) doi:10.1051/0004-6361/201321591 [arXiv:1303.5076 [astro-ph.CO]].
[37] G. Weidenspointner. 1999. The Origin of the Cosmic Gamma-Ray Background in the COMPTEL Energy Range. PhD thesis, Technical University of Munich, Munich, Germany ?id=602832. `http://mediatum.ub.tum.de`
[38] J. Zavala, M. Vogelsberger and S. D. M. White, Phys. Rev. D **81**, 083502 (2010) doi:10.1103/PhysRevD.81.083502 [arXiv:0910.5221 [astro-ph.CO]].
[39] L. E. Strigari, J. F. Beacom, T. P. Walker and P. Zhang, JCAP **0504**, 017 (2005) doi:10.1088/1475-7516/2005/04/017 [astro-ph/0502150].
[40] P. Ruiz-Lapuente, L. S. The, D. Hartmann, M. Ajello, R. Canal, F. K. Ropke, S. T. Ohlmann and W. Hillebrandt, Astrophys. J. **820**, no. 2, 142 (2016) doi:10.3847/0004-637X/820/2/142 [arXiv:1502.06116 [astro-ph.HE]].
[41] S. Horiuchi and J. F. Beacom, Astrophys. J. **723**, 329 (2010) doi:10.1088/0004-637X/723/1/329 [arXiv:1006.5751 [astro-ph.CO]].
[42] A. De Angelis *et al.* [e-ASTROGAM Collaboration], arXiv:1611.02232 [astro-ph.HE].

Appendix: Continuum Photons

Continuum photons affect the CMB by creating spectral distortions [20]. Ref. [38] investigated limits to these spectral distortions modeling the distortions as a Bose-Einstein distribution with a chemical potentioal μ, μ-type distortions. In order to get a baseline estimate on the effect of the continuum photons injected by PBH on the CMB a similar approach was taken. Assuming the injection will alter the perfect blackbody spectrum with the same μ-type distortions, these distortions will be approximately

$$\mu = 1.4\frac{\delta\rho_\gamma}{\rho_\gamma} = 1.4\int_{t_1}^{t_2}\frac{\dot{\rho}_\gamma}{\rho_\gamma}dt, \tag{17}$$

where ρ_γ and $\dot{\rho}_\gamma$ are the energy density of the CMB and the distortion injection rate on the CMB respectfully. $\dot{\rho}_\gamma$ becomes the injection rate directly from the black hole energy going into the continuum. The result is

$$\mu = 1.4\int_{z_1}^{z_2}\frac{(dE/dVdt)_{\rm BH,Cont.}}{\rho_c\Omega_\gamma(1+z)^4}\frac{dz}{(1+z)H(z)}, \tag{18}$$

with $\Omega_\gamma h^2 \sim 2.47\times10^{-5}$.

Current limits on these distortions are $|\mu| < 9.0\times10^{-5}$ at two sigma [38]. A comparison of this constraint and the CMB value discussed in this work is shown in Figure 7. As can be seen, the constraints produced by this work are much stronger, several orders of magnitude, than limits produced assuming a μ-type or similar distortion. The only limits that approache the CMB result are those that consider alterations at extremely late times. These however can be ignored due to CMB photons at this time being much cooler than the 10.2 eV limit for these injections. Thus, the actual alterations at this time is further reduced.

Figure 8 shows a comparison between the results calculated in this work and those from Ref [15]. For low mass PBHs, our work calculates a stronger constaint than the EGB; for larger masses, a weaker constraint is produced. The calculation in Ref [15] has the opposite relationship.

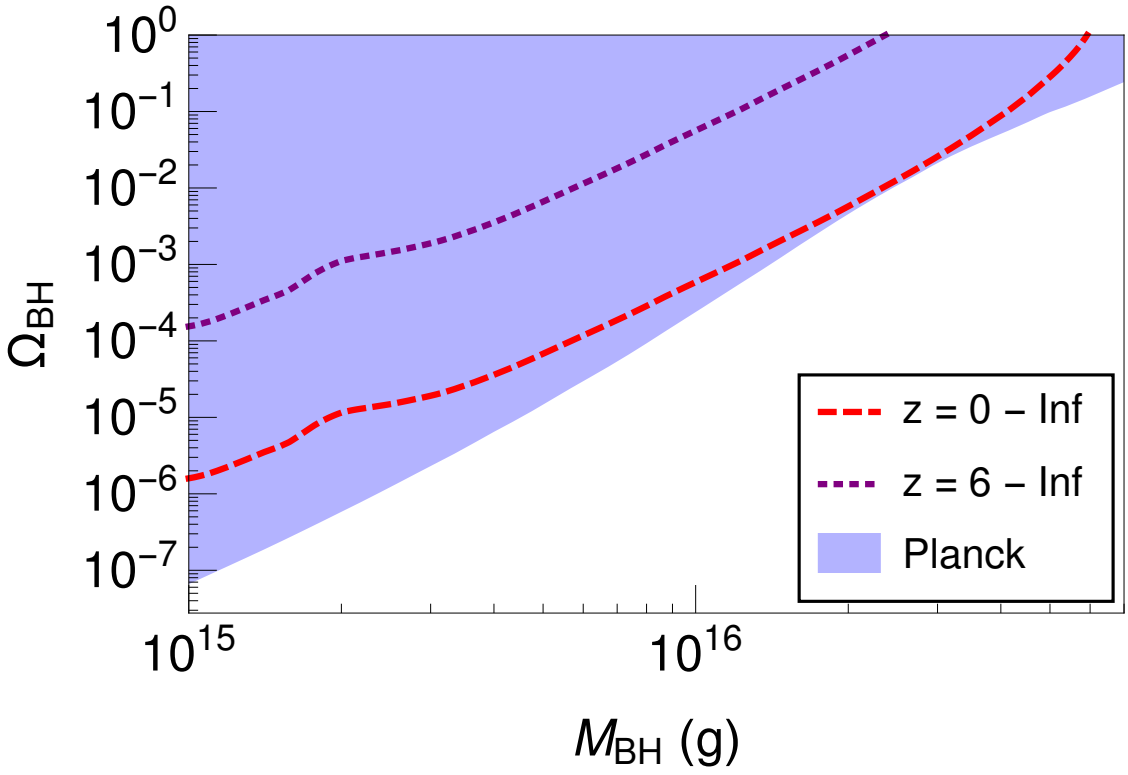

FIG. 7: Exclusion bounds for the fraction of dark matter that can be composed of black holes at the 95% confidence level compared with the same exclusion bound produced through spectral distortions. The various curves correspond to different integration limits in Equation (17). The most constraining uses $z = 0$ to infinity, and the second uses $z = 6$ to infinity.

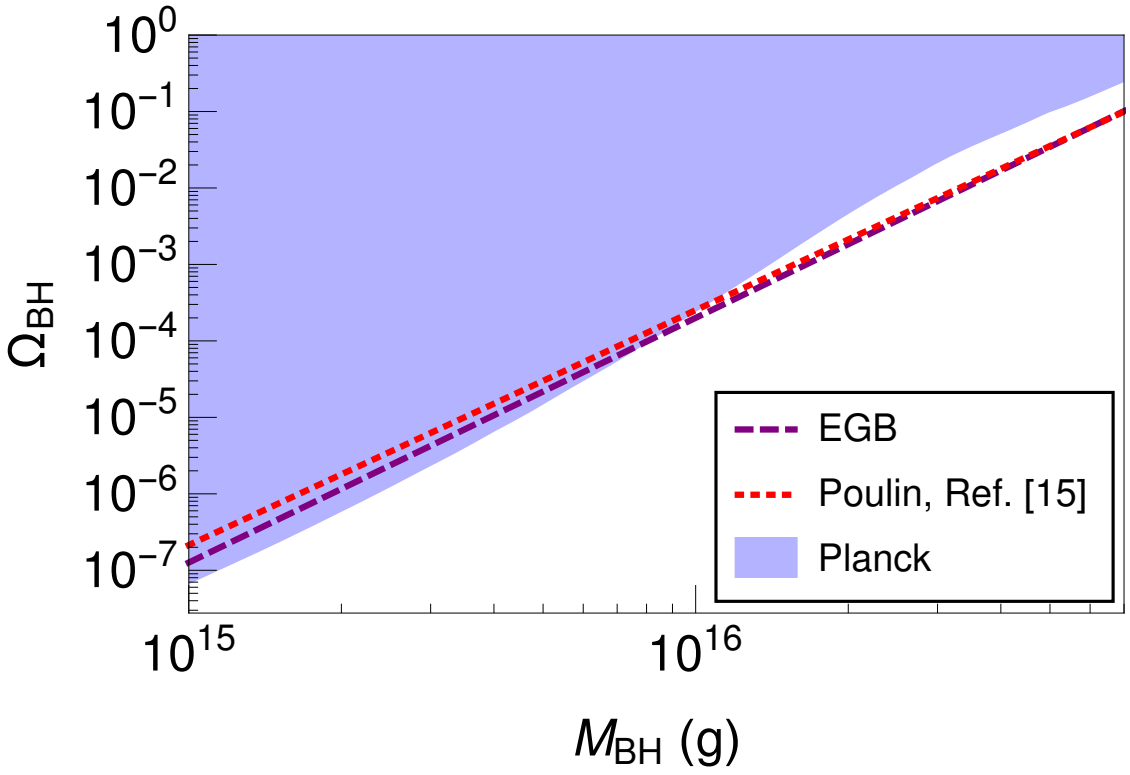

FIG. 8: CMB exclusion bounds for $\Omega_{\rm BH}$ at the 95% confidence level (shaded region) compared with the same exclusion bound enforced by EGB, assuming 100% of the background produced by PBHs (long dashes). Also included is an approximation of the bound found in [15] (long-short dashes).